ARL-CR-0769 • MAR 2015

US Army Research Laboratory

US Army Research Laboratory Materials Center of Excellence

Dynamic Behavior of Noncrystalline and Nanocrystalline Metallic Systems: July 2011–June 2012 Annual Report

edited by KT Ramesh
Recipient Program Manager
Director, Hopkins Extreme Materials Institute
The Johns Hopkins University
Baltimore, MD 21218

and

James W McCauley (Emeritus)
Cooperative Agreement Manager
US Army Research Laboratory
Weapons and Materials Research Directorate, ARL
Aberdeen Proving Ground, MD 21005-5066

under contract W911NF-06-2-0006

NOTICES

Disclaimers

The findings in this report are not to be construed as an official Department of the Army position unless so designated by other authorized documents.

Citation of manufacturer's or trade names does not constitute an official endorsement or approval of the use thereof.

Destroy this report when it is no longer needed. Do not return it to the originator.

ARL-CR-0769 ● MAR 2015

US Army Research Laboratory

US Army Research Laboratory Materials Center of Excellence

Dynamic Behavior of Noncrystalline and Nanocrystalline Metallic Systems: July 2011–June 2012 Annual Report

edited by KT Ramesh
Recipient Program Manager
Director, Hopkins Extreme Materials Institute
The Johns Hopkins University
Baltimore, MD 21218

and

James W McCauley (Emeritus)
Cooperative Agreement Manager
US Army Research Laboratory
Weapons and Materials Research Directorate, ARL
Aberdeen Proving Ground, MD 21005-5066

under contract W911NF-06-2-0006

REPORT DOCUMENTATION PAGE

Form Approved
OMB No. 0704-0188

1. REPORT DATE (DD-MM-YYYY)	2. REPORT TYPE	3. DATES COVERED (From - To)
March 2015	Annual Report	1 July 2011–30 June 2012

4. TITLE AND SUBTITLE

US Army Research Laboratory Materials Center of Excellence

Dynamic Behavior of Noncrystalline and Nanocrystalline Metallic Systems: July 2011 to June 2012 Annual Report

5a. CONTRACT NUMBER
W911NF-06-2-0006

5b. GRANT NUMBER

5c. PROGRAM ELEMENT NUMBER

6. EDITOR(S)
KT Ramesh and James W McCauley

5d. PROJECT NUMBER
BH64

5e. TASK NUMBER

5f. WORK UNIT NUMBER

7. PERFORMING ORGANIZATION NAME(S) AND ADDRESS(ES)
Hopkins Extreme Materials Institute
The Johns Hopkins University
Baltimore, MD 21218

US Army Research Laboratory
ATTN: RDRL-WM
Aberdeen Proving Ground, MD 21005-5069

8. PERFORMING ORGANIZATION REPORT NUMBER

9. SPONSORING/MONITORING AGENCY NAME(S) AND ADDRESS(ES)
US Army Research Laboratory
ATTN: RDRL-WM
Aberdeen Proving Ground, MD 21005-5069

10. SPONSOR/MONITOR'S ACRONYM(S)

11. SPONSOR/MONITOR'S REPORT NUMBER(S)
ARL-CR-0769

12. DISTRIBUTION/AVAILABILITY STATEMENT
Approved for public release; distribution is unlimited.

13. SUPPLEMENTARY NOTES

14. ABSTRACT

This cooperative research program emphasizes collaborative research between The Johns Hopkins University and the US Army Research Laboratory toward well-defined common goals: the understanding and development of advanced lightweight materials for vehicular protection, focusing on high-strain-rate/high-stress testing, determining the operative deformation and failure mechanisms, and developing relevant models to allow for materials design. This report summarizes the research carried out during 1 July 2011 through 30 June 2012 in the following areas: 1) nanomicro aluminum, 2) dynamic failure and damage mechanisms, 3) nanostructured magnesium, 4) modeling of body-centered-cubic nanostructures, 5) high-rate loading of piezoelectric ceramics research thrust, 6) continuum modeling of dynamic deformation mechanisms, 7) density functional theory modeling and transmission electron microscopy characterization of nonstoichiometric oxides and carbides (B_6O_x and B_4C), 8) administration, education, training, and collaborative structures, and 9) list of theses, publications, and presentations from the various thrust areas.

15. SUBJECT TERMS
dynamic properties, nanostructured metals, aluminum, piezoelectricity, BCC metals, modeling, boron carbide and oxide

16. SECURITY CLASSIFICATION OF:			17. LIMITATION OF ABSTRACT	18. NUMBER OF PAGES	19a. NAME OF RESPONSIBLE PERSON
a. REPORT	b. ABSTRACT	c. THIS PAGE	UU	44	James W McCauley
Unclassified	Unclassified	Unclassified			19b. TELEPHONE NUMBER (Include area code) 410-306-0711

Contents

List of Figures

List of Tables

Acknowledgments and Disclaimers

The work contained herein is privileged and may not be reproduced or further distributed without the written permission of the authors. Research was sponsored by the US Army Research Laboratory (Army Robert Morris Acquisition Center - Research Triangle Park [ARMAC-RTP]) and was accomplished under the ARMAC-RTP Cooperative Agreement Number W911NF-06-2-0006. The views and conclusions contained in this document are those of the authors and should not be interpreted as representing the official policies, either expressed or implied, of the US Army Research Laboratory or the US Government. The US Government is authorized to reproduce and distribute reprints for Government purposes notwithstanding any copyright notation thereon.

INTENTIONALLY LEFT BLANK.

1. Introduction

This cooperative research program emphasizes collaborative research between The Johns Hopkins University and the US Army Research Laboratory (ARL) toward well-defined common goals: the understanding and development of advanced lightweight materials for vehicular protection. The Johns Hopkins side of the collaboration is operated through a science-driven, problem-directed center—the Center for Advanced Metal and Ceramic Systems (CAMCS). The research thrusts and the collaborative structures of the Center provide a basis for the substantial enhancement and continuous improvement of the scientific and technical capabilities of ARL, and particularly of the Weapons and Materials Research Directorate (WMRD).

This document is an annual report for research performed in the last six months of the calendar year (CY) 2011 and the first 6 months of the calendar year 2012. Each research thrust operates a Collaborative Research Group, or CRG, with joint responsibility for the development of the research. The next few pages present individual reports for each research thrust during the period indicated above. Where revised objectives are presented, these have been discussed and approved by the CRG unless otherwise indicated. Note also that the ARL collaborators listed represent all individuals who have indicated a desire to be involved in each thrust area (the lead ARL collaborator is identified in italics).

Note that the core Materials Center of Excellence program was in a transition phase in 2012, with a 50% budget reduction in CY 2012. The 2012 effort therefore focused on wrapping up graduate student work while transitioning data, techniques, and models.

2. Nanomicro Aluminum Research Thrust

Core Faculty: KT Ramesh, KJ Hemker

ARL Collaborators: K Cho (lead). *Interest Group:* ESC Chin, J Beatty, G Gazonas, K Doherty, J McCauley, RJ Dowding, A Cho, B Cheeseman

Graduate Student: Emily Huskins

2.1 Long-Range Objectives

The long-range objectives of this study are as follows:

- Determine the deformation and failure mechanisms in nanomicro aluminum (Al) alloys and their composites subjected to impact rates of loading.
- Develop models for the dynamic deformation and dynamic failure of nanomicro composites, with the objective of enabling materials design.

2.2 Objectives for July 1, 2011, to June 30, 2012

Third Quarter 2011:

- Determine implications of model for stability of high-strength Al alloys during dynamic deformations; compare 2139 Al and ultra-fine-grained (UFG)/nano-Al
- Begin experiments to measure dynamic tensile ductility and dynamic damage processes in high-strength Al alloys

Fourth Quarter 2011:

- Continue experiments to measure dynamic tensile ductility and dynamic damage processes in high-strength Al alloys

First Quarter 2012:

- Internal variable model for evolution and stability of high-strength Al alloys during dynamic deformations

Second Quarter 2012:

- Handoff improved strengthening model for 2139 Al to US Army Research Laboratory collaborators
- Complete doctoral dissertation (Huskins)

2.3 Research Summary

A physics-based thermo-mechanical-viscoplastic model with 2 internal state variables was constructed. The thermo-elasto-viscoplastic constitutive equation and flow rule were developed using internal state variable theory for 3-dimensional (3-D) finite deformation of isotropic, pure, UFG face-centered cubic (FCC) metals. Two scalar internal state variables were selected: the total dislocation density and the average grain size. The strain rate and temperature dependence of the deformation is captured in the flow rule through the equivalent plastic strain rate function. The functional forms of the constitutive equation, flow rule, and internal state variable evolution equations are thermodynamically consistent. In this constitutive formulation, viscoplasticity is modeled without a defined yield function. The following mechanisms are accounted for in the model:

- Temperature, strain rate, and grain size effects
- Evolution of dislocation density during deformation
- Evolution of grain size during deformation
- Evolution of temperature during deformation
- Static evolution of internal state variables prior to loading.

The viscoplastic flow rule is written as

$$\mathbf{D}^P = \dot{\bar{\epsilon}} \frac{3\tilde{\boldsymbol{\sigma}}'}{2\bar{\sigma}} \,, \tag{1}$$

where the equivalent plastic strain rate is

$$\dot{\bar{\epsilon}}^P = f\left(\bar{\sigma}, T, \rho, d\right), \tag{2}$$

defined as a function of the equivalent stress ($\bar{\sigma}$), temperature (T), and the internal state variables, total dislocation density (ρ), and average grain size (d). The inverse of Eq. 2 is the scalar viscoplastic flow law.

The scalar thermo-viscoplastic constitutive model consists of Eqs. 3–6:

The scalar viscoplastic flow law,

$$\bar{\sigma}\left(\dot{\bar{\epsilon}}^P, T, \rho, d\right) = \hat{\sigma}_a\left(d\right) + \hat{\sigma}_t\left(\rho\right) \frac{\mu(T)}{\mu_o} \left[1 - \left[\frac{kT}{\mu(T) b^3 g_o} \ln\left(\frac{\dot{\epsilon}_o^P}{\dot{\bar{\epsilon}}^P}\right)\right]^{1/q}\right]^{1/p} . \tag{3}$$

The athermal deformation resistance is a modified Hall-Petch term,

$$\hat{\sigma}_a := k_y' d^{-1/2} \,, \tag{4}$$

and the thermal deformation resistance is

$$\hat{\sigma}_t := \alpha M \mu_o b \sqrt{\rho} \cdot \tag{5}$$

The second term in Eq. 3 contains the stress dependence of the temperature, strain rate, and 2 internal state variables.

The evolution equation for the dislocation density internal state variable is

$$\dot{\rho} = M\dot{\bar{\epsilon}}^P \left(\frac{\beta_1 \left(\dot{\bar{\epsilon}}^P\right) \sqrt{\rho}}{b} + \frac{\beta_2}{bd} - \kappa \left(\dot{\bar{\epsilon}}^P, T, d\right) \rho \right) - r\left(T, \rho\right), \tag{6}$$

where κ is defined as

$$\kappa \left(\dot{\bar{\epsilon}}^P, T, d\right) = \frac{\beta_1 \left(\dot{\bar{\epsilon}}^P\right)}{b\sqrt{\rho_s \left(\dot{\bar{\epsilon}}^P, T, d\right)}} + \frac{\beta_2}{bd\rho_s \left(\dot{\bar{\epsilon}}^P, T, d\right)}, \tag{7}$$

and the saturation dislocation density is a function of grain size, temperature, and strain rate as

$$\sqrt{\rho_s \left(\dot{\bar{\epsilon}}^P, T, d\right)} = h\left(d\right) \rho_{so} \left(1 + \left(\frac{\dot{\bar{\epsilon}}^P}{\dot{\bar{\epsilon}}^P_{os}} \right)^{N(T)} \right). \tag{8}$$

Three components of dislocation density evolution are included: a static component in which static recovery occurs during preheating, a source term by which the dislocation density increases during deformation, and a dynamic recovery term by which dislocation annihilation through mechanisms such as cross-slip reduce the dislocation density during deformation.

The evolution equation for the grain size internal state variable is

$$\dot{d} = \dot{d}_{stat}\left(T, d\right), \tag{9}$$

accounting for static grain growth during preheating, prior to loading.

The evolution equation for the temperature is

$$\dot{T} = \frac{\omega}{\rho_m C_v} \bar{\sigma} \dot{\bar{\epsilon}}^P, \tag{10}$$

such that the temperature increases as a result of plastic strain.

Model parameters were obtained from a combination of data within the literature and data obtained through high-strain-rate, high-temperature experiments on UFG Al-1100. Calculations were performed for both static and dynamic heating conditions such that the effects of preheating prior to loading during realistic laboratory experiments are accounted for.

The effects of preheating are shown through a series of high-temperature calculations at a strain rate of 7,000 s^{-1} in which the static components of the evolution equation vary. In all calculations the initial grain size is 500 nm and initial dislocation density is 2×10^{14} m^{-2}. Solid lines in both Figs. 1.1a and b include both static recovery and static grain growth terms. In Fig. 1a the dashed lines represent the case of fixed grain size (no static grain growth), while in Fig. 1.1b the dislocation density is fixed (no static recovery). From these figures it is evident that the decrease in flow stress which occurs because of static grain growth is significant, while the influence of static recovery is only evident at the highest temperature.

(a)

(b)

Fig. 1.1 Computer stress-strain curves for UFG Al-1100 at 7,000 s^{-1} including static recovery and static grain growth (solid lines), a) excluding static grain growth (dashed lines) and b) excluding static recovery (dashed lines)

Figure 1.2 shows the predicted thermal softening behaviors at a strain rate of 7,000 s^{-1} of 3 different Al-1100 materials (solid markers) in comparison with

experimental data (open markers). Calculations were performed for 3 model materials: a coarse-grained (CG) Al-1100, an UFG Al-1100 in which preheating was simulated from the static evolution terms, and an UFG Al-1100 without simulating preheating. The experimental data for UFG without preheating was obtained through Cottrell-Stokes-type experiments. From Fig.1.2 it is evident that predicted thermal softening behavior of both CG and UFG materials at high strain rates are consistent with experimentally observed trends.

0.3

Fig. 1.2 Model predictions for thermal softening of UFG Al-1100 (solid markers) compared with experimental data on UFG and CG Al-1100 (T_m is the melting temperature)

2.4 Collaborative Interactions

Collaborations continue with Profs J Schoenung and E Lavernia of UC Davis on Al-5083-based nanomicro materials.

2.5 Publications and Presentation

1. Huskins EL, Cao B, Li B, Ramesh KT. Temperature-dependent mechanical response of an UFG aluminum alloy at high rates. Experimental Mechanics. 2012;52:185–194.

2. Huskins EL, Ramesh KT. Microstructure evolution of UFG Al-1100 during high temperature kolsky bar experiments. Session: novel testing techniques II, SEM International Congress. 2012 Jun 11–14; Costa Mesa, CA.

2.6 Student Theses/Dissertations/Graduations

1. Huskins EL. The thermo-mechanical response of UFG aluminum at high strain rates. [dissertation]. [Baltimore (MD)]: The Johns Hopkins University; 2012.

2. Huskins EL, PhD in Mechanical Engineering, date conferred 2012 Aug 31.

3. Dynamic Failure and Damage Mechanisms Research Thrust

Core Faculty: KT Ramesh, L Graham-Brady, K Hemker

ARL Collaborators: J McCauley (lead). *Interest Group:* K Cho, BE Schuster, RH Kraft, J Beatty, ESC Chin, G Gazonas, L Kecskes, T Weerasooriya, L Magness, S Schoenfeld, RJ Dowding, T Sano, T Bjerke, D Casem

Postdoctoral Research Fellow: Dr Nitin Daphalapurkar

Graduate Students: Cindy Byer, Guangli Hu

ARL Graduate Student: Cyril Williams

3.1 Long-Range Objectives

The long-range objectives of this study are as follows:

- Characterize micromechanisms of dynamic deformation and failure developed within the other Center for Advanced Metallic and Ceramic Systems (CAMCS) thrusts.
- Develop physics-based models for the massive failure of lightweight metallic systems.
- Develop mechanism-based models for the evolution of damage within heterogeneous materials under dynamic loading.

3.2 Objectives for July 1, 2011, to June 30, 2012

Third Quarter 2011:

- Continue development of mechanism-based multiscale approach to microstructure design for dynamic applications.
- Understand mechanics of twinning and size in magnesium.

Fourth Quarter 2011:

- Continue development of mechanism-based multiscale approach to microstructure design for dynamic applications.
- Complete doctoral dissertation (Williams).

First Quarter 2012:

- Complete doctoral dissertation (Williams).

- Transition the BCC crystal plasticity effort to Dr Daphalapurkar.

Second Quarter 2012:

- Incorporate source statistics into crystal plasticity models of magnesium micro-pillars.
- Complete doctoral dissertation of Guangli Hu on modeling of dynamic failure of advanced ceramics.

3.3 Research Summary

3.3.1 Kinetics of Fast-Moving Twin Boundaries

We provide a kinetic relation for a moving twin boundary (TB) in nickel (Ni) for a wide range of shear stress values (from a few 5 MPa to 11 GPa). We obtain TB velocities at stress levels that are accessible to plate-impact experimental techniques as an example. To our knowledge the results on TB motion reported in the literature have focused only on the kinematics aspects of motion and were restricted to very high shear stresses (>7 GPa in Ni). In addition, for the first time, the kinetics of a twinning partial dislocation is reported. The use of a tall specimen geometry prevents a moving TB from interacting with the stress waves (reflected from the boundary of a specimen) and achieves steady-state velocities of propagation.

The following results were demonstrated:

- The velocities of a moving TB tend to saturate (at 700 m/s) well below the shear-wave speed in Ni. This has implications for modeling dynamic response of metals (e.g., nanotwinned and nanocrystalline) undergoing plastic deformation—specifically, the viscous drag term can become important for twin boundaries that move under certain loading conditions.
- The kinetics of a propagating twinning partial dislocation is fundamental to TB motion. We propose a kinetic relation which can act as an input in continuum and dislocation dynamics models for a moving TB.
- The novel methodology described in this work can be used to extract a kinetic relation for TB motion in the presence of a twinning partial dislocation.
- TB motion in the propagation regime suggests a size dependence (twin-length/specimen width/grain-size) and suggests a source of softening mechanism that has not been accounted for before.

Finally, results from molecular dynamics can be used to guide the design of experiments (e.g., plate impact) for validation of the kinetic relation.

3.3.2 Specimen Size Effects on the Dynamic Failure Strength of Brittle Materials

From available options, a common approach to subjecting a specimen to increasing strain rates (in a Kolsky bar setup) is to decrease the specimen size.

Typical specimen sizes of 0.8–1 mm are being used to obtain rates on the order of 10^4/s in a Desktop Kolsky Bar (DKB) setup. In this study, we interrogate the effect of surface flaws with reducing specimen sizes in terms of the dynamic failure pattern and the dynamic failure strength.

In Table 3.1, we summarize effects of reducing the specimen size:

Table 3.1 Effects of reducing specimen size

Parameter	Dynamic Failure Strength	Equation
Maximum flaw size ↓	↑	Weibull (1951) Weakest-link theory
Sampling ↑ (same maximum flaw size)	↑	Graham-Brady et al. IJSS (2011) Daphalapurkar et al. JMPS (2011)
Strain Rate ↑	↑	Kimberley et al. (under review)
Spatial heterogeneity of the damage	No change at high rates	Daphalapurkar et al. JMPS (2011)

However, all of the above-mentioned effects are attributed to the bulk flaws, and none of them can describe a decrease in the failure strength that was observed for specimens tested using the DKB (Guangli Hu et al., ICACC, Daytona, FL, 2011). In this work, we use a computational approach to perform dynamic fracture simulations of idealized specimens with a certain density of surface flaws. A procedure detailed in Daphalapurkar et al. (JMPS, 2011) is used to carry out dynamics fracture simulations using the cohesive zone model, as illustrated in Fig. 3.1. Following are the important length and time scales relevant to these simulations:

Length Scales	Time Scales	Surface flaws
Mesh size: 2.5 μm Cohesive zone length (l_c): 5 μm Flaw spacing: 25 μm Specimen length (h): 0.1-1 mm	Strain rate: 10^4 /s Time step: 1 ps	Linear density: 8 flaws/mm Size: 20 μm

Fig. 3.1 Effect of reducing specimen size on the failure pattern (on left) and the dynamic failure strength (on right) under tension

3.4 Summary

- Low dynamic failure strengths for reduced specimen sizes may be attributed to the influence of surface flaws.
- Simulations suggest a limiting ratio for surface flaw size to specimen size.
- Below a certain critical ratio (surface flaw size to the specimen size), the strength reduces.
- Smaller specimen sizes for DKB would require a stringent control on machining (limiting allowable flaw sizes on the surface).

3.5 Collaborative Interactions

McCauley J, Gazonas G, and others during CAMCS/US Army Research Laboratory Collaborative Research Group meetings that took place every 2 months.

3.6 Publications and Presentations

Daphalapurkar NP, Wright TW, Ramesh KT. Dynamics of twin boundary motion in face-centered cubic metals. SES. 2011 Oct; Evanston, IL.

Daphalapurkar NP, Hu G, Ramesh KT. Specimen size effects on the dynamic failure strength of brittle materials. ICACC. 2012 Jan; Daytona, FL.

Daphalapurkar NP, Wright TW, Ramesh KT. Kinetics of moving twin boundaries. TMS. 2012 Mar; Orlando, FL.

Daphalapurkar NP, Ramesh KT. Orientation dependence of the nucleation and growth of partial dislocations and possible twinning mechanisms in aluminum. J Mech. Phys. Sol. 2012;60:277–294.

Daphalapurkar NP, Ramesh KT. Designer materials for a secure future. Peer-Reviewed Conference Proceeding Paper. Defense, Security and Sensing, SPIE, 2012.

Daphalapurkar NP, Wright TW, Ramesh KT. Manuscript for submission to Physical Review Letters: Kinetics of a fast moving twin boundary.

3.7 Student Theses/Dissertations/Graduations

Williams C. PhD in Mechanical Engineering, date conferred 2012 May 21.

4. Nanostructured Magnesium Research Thrust

Core Faculty: KT Ramesh

ARL Collaborators: S Mathaudhu (lead). *Interest Group*: RJ Dowding, J Beatty, L Kecskes

Graduate Student: Cindy Byer

4.1 Long-Range Objectives

The long-range objectives of this study are as follows:

- Determine the potential of nanostructured magnesium (Mg) alloys for vehicle applications.
- Examine the issues of formability and corrosion resistance of nanostructured Mg alloys and their composites.

4.2 Objectives for 2011

4.2.1 Third Quarter 2011

- High-strain-rate evaluation (Kolsky bar rates) of ball-milled Mg produced by Darling et al.

4.2.2 Fourth Quarter 2011

- High-strain-rate-evaluation (Kolsky bar rates) of ultra-fine-grained and nanocrystalline Mg produced by the US Army Research Laboratory (ARL) and other collaborators.

4.3 Research Summary

No ball-milled Mg materials produced by ARL were evaluated, since they were not available at the time. However, we examined fine-grained Mg provided by ARL using the Kolsky bar to examine the development of texture and twinning.

4.4 Publications and Presentations

None.

5. Modeling of Body-Centered-Cubic (BCC) Nanostructures Mod

Core Faculty: KT Ramesh

ARL Collaborators: William de Rosset, Brady Butler, Eric Klier

Postdoctoral Fellow: Swapnil Patil

5.1 Long-Term Objectives

The focus is on the mesoscale modeling of body-centered-cubic (BCC) nanomaterials with nanomicro microstructures. The global objective is to provide guidelines for microstructural design to optimize the mechanical properties and to control the failure, with the emphasis on those properties and processes that are unique to BCC materials. The approach is to use mesoscale and crystal plasticity simulations to understand deformation and failure processes.

5.2 Quarterly Deliverables: Objectives for July 1, 2011, to June 30, 2012

Third Quarter 2011:

- Implement strain-gradient crystal plasticity to model grain-size effect in polycrystalline BCC metals.

Fourth Quarter 2011:

- Demonstrate simulations of polycrystalline microstructure using the strain-gradient crystal plasticity model.

First Quarter 2012:

- Calibrating properties assigned at the slip-system level for simulating single-crystal plasticity of molybdenum (Mo); modeling the tension-compression asymmetry of the stress-strain response in Mo (under the quasi-static rates of loading).

Second Quarter 2012:

- Comparing the stress-strain curve for Mo using a separate validation experiment (compression of a plate with a hole).

5.3 Research Summary

5.3.1 Strain Gradient Crystal Plasticity (SGCP)

The following list summarizes our results on strain gradient crystal plasticity:

- Enhanced the BCC 2- and 3-dimensional (2-D and 3-D) crystal plasticity model, incorporating strain gradient effects to simulate polycrystalline microstructures.
- Introduced 2 material length scales to model the influence of reducing grain size on the plastic flow in BCC polycrystalline metals.
- Conducted a preliminary study demonstrating size effects in Mo from simulations.
- Demonstrated, for the future work, the necessity of 3-D computations to correctly capture the 3-D nature of tensorial stress and gradient effects. We also demonstrated the need for a better model to determine the back stress in the strain gradient crystal plasticity (SGCP) model.

Figure 5.1 shows numerical simulation results using the 2-D SGCP from a uniaxial test on a polycrystalline Mo specimen. Contour snapshots from the simulation (at an in-between time) are shown for geometrically necessary dislocation density (simulating dislocation pilling at the grain boundaries), effective plastic strain, and the normal stress component (simulating heterogeneity bands of stress that eventually lead to shear-banding). The stress-strain plot shows how the length scale parameter (L) can be adjusted to match the experimental stress-strain curve. One of the critical issues with the 2-D plane strain SGCP simulations is that the gradients in the out-of-plane direction are not simulated. This introduces an error in back stress computation; it also affects the convergence of the finite element solution. From a separate set of calculations, we additionally conclude that 3-D numerical simulations will significantly reduce the above-mentioned errors.

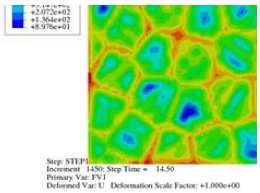

Fig. 5.1 Polycrystalline simulations using 2-D strain-gradient crystal plasticity

5.3.2 Validation of Single-Crystal Plasticity Parameters for Mo

A single-crystal plasticity framework for BCC was developed as part of the previous year's effort, and this part of the code has been handed over to the US Army Research Laboratory (ARL) (J McCauley, W de Rosset, H Maupin, on 17 Oct 2012 by N Daphalapurkar). Since then, advancements in the model include implementation of strain gradient crystal plasticity; Section 5.3.1 shows representative results from simulations.

In the later part of this study, we focused our efforts on validating the Mo fitting parameters. To simulate Mo, the material parameters at the slip system level were calibrated to reproduce the experiments on Mo under tension at different temperatures. The motivation behind this effort was to revisit the calibration of BCC single-crystal parameters at the slip system level, perform a higher-level validation study, and perform simulations for a wide range of experimental variables, including experiments for 2 different stress states (uniaxial tension and compression) and additionally for different temperatures.

Outcome: In order to better match the simulation results with the experiments (to capture the tension-compression symmetry), we reduced the constraints on the slip systems that model latent hardening between different slip systems. Following are the new set of equations that describe the stress update for individual slip systems:

$$\dot{g}^{\alpha} = \sum_{\beta=1}^{n} h_{\alpha\beta}\dot{\gamma}_{\beta}$$

$$h_{\alpha\beta} = h_{\alpha} q_{\alpha\beta} \quad (\text{no sum})$$

$$h_{\alpha} = h_{s} + (h_{i} - h_{s})\, sech\left[\frac{(h_{i} - h_{s})}{(g_{s} - g_{o})}\gamma_{\alpha}\right]^{2} \quad ,$$

where g_{α} is the athermal slip resistance, h_{α} vs. γ_{α} is the flow law in shear for individual slip systems, and $q_{\alpha\beta}$ is the latent hardening matrix.

The BCC crystal plasticity framework and calibration of the material parameters at the slip system level were tested by performing a validation experiment in which the specimen experiences a heterogeneous stress state. A single-crystal Mo specimen with a hole was subjected to compression at a quasi-static rate. The stress-strain result from simulation was compared to that from the experiment, shown in Fig. 5.2 (bottom right).

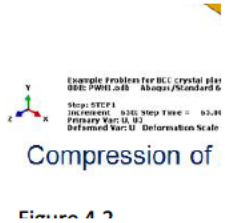

Fig. 5.2 Single-crystal plasticity stress-strain curves fitted to experiments on single-crystal Mo (top). Simulated compression of a specimen with a hole (bottom left), under compression at quasi-static rate. Comparing results from simulations with experiments (bottom right).

Summary: We have a fair comparison of simulation results with experiments. Our conjecture is that the experimental results in the literature (used to calibrate the material parameters) have differences in their stress-strain curves. Mo—being sensitive to temperature, strain rates (even at low rates), and impurity levels—adds to the complexity of comparing different experimental results. Additionally, experiments themselves may have variability in their results. These sources of variability need to be accounted for while calibrating the material parameters in the model. One option is to calibrate the model material parameters based on a statistically representative set of curves from experiments (that would account for variability).

5.4 Collaborative Interactions

William de Rosset (ARL) and Swapnil Patil (formerly at The Johns Hopkins University [JHU]). Swapnil Patil (formerly at JHU) with Nitin Daphalapurkar for transfer of software and knowledge base.

5.5 Publications and Presentations

Manuscript in preparation for submission to Acta Materialia: Daphalapurkar NP, Patil S, Ramesh KT. On modeling BCC crystal plasticity: application to molybdenum.

6. High-Rate Loading of Piezoelectric Ceramics

Core Faculty: KT Ramesh

ARL Collaborators: George Gazonas, Jim McCauley

Postdoctoral Fellow: Leslie Lamberson

6.1 Objective

Understand the coupling between the dynamics of loading and the piezoelectric behavior of a model ceramic (e.g., silicon carbide [SiC], quartz, or aluminum nitride) using both experiments and modeling. This work may take advantage of interactions with Penn State University's work on piezoeltromagnetic coupling in ceramics.

6.2 Quarterly Deliverables

Third Quarter 2011:

- Perform plate impact experiments on cultured quartz, and possibly a single-crystal SiC sample to probe higher strain rate behavior.

Fourth Quarter 2011:

- Analyze the interaction between loading dynamics and the electromechanical coupling: establish relevant length and time scales for response.

First Quarter 2012:

- Perform Kolsky experiments on single-crystal SiC with simultaneous measurement of electrical and deformation fields.

Second Quarter 2012:

- Working with Prof Trolier-McKinstry of Penn State to analyze the interaction between loading dynamics and the electromechanical coupling in single-crystal SiC.
- Put together archival journal publication summarizing these results.

6.3 Research Summary

Model ceramics of single-crystal quartz and SiC have been experimentally investigated to gain a fundamental understanding of coupled-field problems under

dynamic loading regimes. As a result, an empirical methodology to quantify the dynamic electromechanical behavior of single crystals was fully developed on the Kolsky bar apparatus for quartz and then extended to SiC.

The electrical response from dynamic compression tests on x-cut single-crystal α-quartz specimens impacted normal to the second-order prism or [11$\bar{2}$0] plane at strain rates of 10^3 s^{-1} indicate dissimilar stress-charge behavior during damage evolution. Specifically, when quartz is undergoing extensive and irreversible dynamic brittle fracture under a compressive stress impulse of up to 2 GPa, the effective piezoelectric strain coefficient (d_{11}) exhibits, on average, an approximate 15% increase from loading to unloading. The enhanced piezoelectric behavior during unloading appears to be driven predominantly by the nominal crack density and does not appear to be driven by inertial or rate effects under these loading conditions. Interrupted dynamic tests on single-crystal quartz (Fig. 6.1) appeared to corroborate this finding, where increasing piezoelectric performance is shown even with discontinuous dynamic impact damage to failure. One possible reason for the resulting augmentation of the piezoelectric strain coefficient could be due, in part, to the dielectric breakdown of air as it enters the material system (via cracks) during the fragmentation process. The results for quartz have also revealed clear preferential dynamic failure planes along the second-order trigonal pyramidal [11$\bar{2}$2] plane.

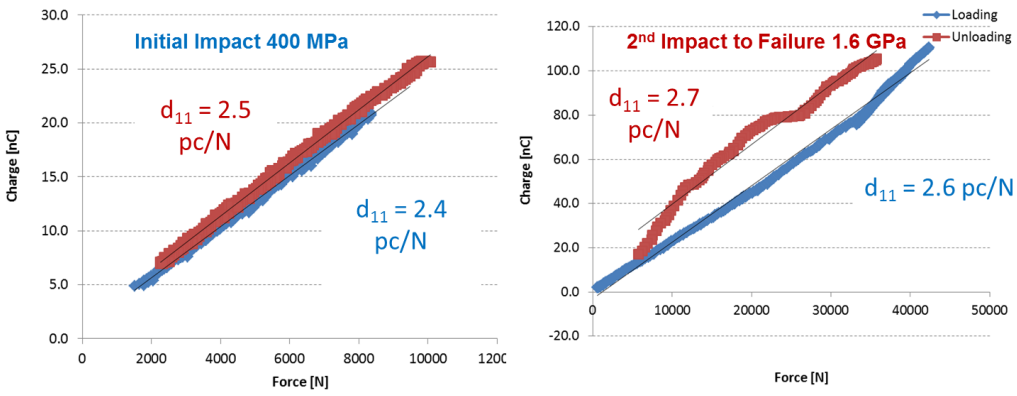

Fig. 6.1 Interrupted dynamic test on single-crystal quartz. Left image shows initial impact to 35% damage, load and unload curves illustrating the piezoelectric coefficient only slightly increasing. Right image shows the consequent impact that completely fails the specimen (100% damage). Here the piezoelectric coefficient shows substantial increase on the unloading portion (top line) of the dynamic response.

The electrical response from dynamic compression tests on single-crystal SiC (6H) and (4H) impacted normal to the basal or [0001] plane at strain rates of 10^3 s^{-1} exhibited a highly varying piezoelectric response during loading and runaway

conductivity when reaching the peak stress, possibly due to the breakdown or short circuit of the electrodes. The failure process of SiC was more rapid than quartz and could be due to the fact that these tests impacted a different crystallographic loading plane than quartz and had a different chemical composition. In general, at equivalent strain rates the SiC samples exhibited faster axial crack speeds of approximately 0.7 C_R, or 70% of the Rayleigh wave speed, whereas the quartz exhibited 0.3 C_R on average. The high variation in the dynamic electromechanical response of SiC is speculated to be caused by the greater number of impurities or flaws in the microstructure of the samples, combined with the relatively small band gap that allows electrons to move relatively freely about the system. General computational SiC literature lists the piezoelectric coefficient of (6H) along the basal plane from roughly 0.2 to 0.6 pC/N. During loading, the (4H) discernible data tended to range roughly from 0.15 to 0.25 pC/N. In addition, the pure mechanical response of the single crystals was also assessed in the quasi-static and dynamic regime for a baseline prior to electromechanical studies. In the limited number of quasi-static mechanical tests, both (6H) and (4H) appeared to withstand slightly higher compressive loads with less variation than in dynamic loading conditions, approximately 3 GPa. Overall, dynamic compressive tests showed that (6H) SiC was able to withstand 22% higher dynamic compressive stress before failure than (4H). Of 6 tests of each sample performed at 10^3 s^{-1}, the (6H) samples averaged a dynamic compressive strength of 2.7 GPa (standard deviation of 400 MPa), and the (4H) samples averaged 2.0 GPa (standard deviation of 260 MPa).

6.4 Publications and Presentations

Lamberson et al. Damage and the electromechanical behavior of piezoelectric ceramics. SEM Annual Meeting, Jun 2012.

7. Continuum Modeling of Dynamic Deformation Mechanisms

Core Faculty: KT Ramesh

ARL Collaborators: J McCauley

Adjunct Research Professor: TW Wright

7.1 Objective

Examine the nonlinear constitutive characteristics of boron carbide (B_4C) from the point of view of Continuum Mechanics in order to provide guidance for fundamental density functional theory (DFT) studies of material instability. Because elastic strain has 6 independent components, a general constitutive representation for B_4C should limit the number and types of applied strain paths required for a full understanding of material instability.

7.2 Quarterly Deliverables

Fourth Quarter 2011:

- Continued development of a model for the amorphization of B_4C under combined loading from pressure and shear.

7.3 Research Summary

A general framework for elastic nonlinear constitutive representations was developed from a modified version of the known Voigt matrices of linear elastic moduli for materials of any symmetry. Each frame is constructed from the eigenvalues and eigentensors of the modified Voigt matrix for linear materials of a particular symmetry, and it is shown that the frame is valid for both linear and nonlinear materials of that symmetry. Building on previous work concerning the nonlinear representations, we attempted to construct minimal nonlinear representations for all symmetries.

7.4 Collaborative Interactions

This work was conducted in a collaborative effort with Dr James McCauley and Dr DeCarlos Taylor of the US Army Research Laboratory, who provided materials science and DFT calculations, respectively, for the broader study.

7.5 Publications and Presentations

1. Wright TW. Bootstrap elasticity: from linear to nonlinear constitutive representations. Journal of Elasticity. 2012;109;(1)35–49.

2. Taylor DE, Wright TW, McCauley JW. First principles calculation of stress induced amorphization in armor ceramics. Aberdeen Proving Ground (MD): Army Research Laboratory (US); 2012 Mar. Report No.: ARL-TR-5966.

3. Wright TW. Nonlinear elastic constitutive representations. Presented at Society of Engineering Science, 2011 Oct; Evanston, IL.

4. Wright TW. Nonlinear anisotropic elasticity: guide for exploring stability in pressure/shear. Presented at the American Physical Society, 2012 Feb; Boston, MA.

8. Density Functional Theory (DFT) Modeling and Transmission Electron Microscopy (TEM) Characterization of Nonstoichiometric Oxides

JHU Faculty: Kevin Hemker

JHU Postdoctoral Fellows: Dr Changqiang Chen and Dr Kelvin Xie

Consultant: John Smith

ARL PoC: Gary Gilde, and Jennifer Dunn, Todd Beaudet, Betsy Rice, Jerry LaSalvia, Bob Pavlacka, Gene Shanholtz, Steve Kilczewski, Gary Gilde, Betsy Rice, Jim McCauley

8.1 Long-Term Objectives

Nonstoichiometric oxides and carbides of boron suboxide (B_6O), boron carbide (B_4C), and aluminum oxide (Al_2O_3) offer considerable promise as armor materials and are under development at the US Army Research Laboratory (ARL). Density Functional Theory (DFT) models are being developed to guide the development of processing routes, and detailed atomic-level characterization is needed to support these models. Dr John Smith, a widely recognized expert in DFT modeling, will serve as a consultant. The experimental objectives of this study will be to prepare transmission electron microscopy (TEM) specimens and characterize nonstoichometric oxides and carbides currently under development at ARL. We will start with B_6O_x, but extensions to B_4C and Al_2O_3 are envisaged. Conventional electron microscopy and high-resolution imaging (HRTEM), electron energy loss spectra, energy-filtered imaging, and aberration-corrected high-angle annular dark field scanning transmission electron microscopy will be employed to assess grain morphology, grain boundary phases and chemistry, crystallographic texture, and fractional atomic coordinates and atomic occupancies.

8.2 Quarterly Deliverables

Fourth Quarter of 2012:

- Review literature on the liquid phase sintering and grain boundary engineering in silicon carbide, B_4C, and B_6O.
- Conduct initial sintering work on B_4C and B_6O with silicon dioxide (SiO_2) as additive with mechanical property tests and TEM characterization.

8.3 Research Summary

8.3.1 Experiment

Consolidated B_4C, B_4C with 5% SiO_2, and B_6O were successfully sintered at ARL. The B_4C specimen was sintered at 1,800 °C, while the B_4C with 5% SiO_2 specimen was sintered at 1,750 °C. All the consolidated ceramics are fairly dense, however, with some microscale voids present within the structure for all specimens. In the B_4C specimen, conventional TEM micrographs revealed that there are also some nanoscale pores between the grains. The grain boundaries were clean. In the B_4C with 5% SiO_2 specimen, there was no intergranular film constituting Si-rich phase observed using both conventional TEM and HRTEM, as shown in Figs. 8.1a and b. Energy dispersive x-ray spectroscopy revealed no substantial difference in Si contents within the grains and at the grain boundaries. This further suggested the absence of intergranular film at grain boundaries. Interestingly, amorphous Si-rich pockets were observed to fill up some of the nanopores, as shown in Figs. 8.1a and c. These observations suggested that there was no wetting between SiO_2 and B_4C during the sintering process, and the glassy Si-rich phase aggregated at the triple points between grains. TEM studies were also carried out in the consolidated B_6O specimen. The specimen possessed a biomodal structure with some grains tens of microns in size and other grains only approximately 500 nm. Iron (Fe), chromium (Cr), nickel (Ni), manganese (Mn), tungsten (W), magnesium (Mg), and aluminum (Al) were identified as impurities in the materials and were believed to be introduced into the material during processing. Again, careful tilting experiments in TEM using HRTEM imaging showed no intergranular film at grain boundaries, and impurities aggregated at triple points of B_6O grains.

Fig. 8.1 a) Bright-field TEM micrograph that shows the microstructure of a consolidated B_4C with Si as additive. b) and c) are HRTEM images taken from the areas indicated by red circles in a). b) HRTEM micrograph of a grain boundary triple point. No amorphous layer of silicon was observed. * marks the grain boundaries between the 3 grains. c) An amorphous silicon phase was observed to fill the pores of B_4C.

8.3.2 Theory

The program goal is to improve the fracture toughness of B_4C as a potential material for lightweight armor. Insights for this can be gained at the atomistic level and from first principles via DFT. Initial DFT results for B_4C are presented here. $B_{11}C_pCBC$ was found to be the lowest energy bulk polytype. Promoting intergranular fracture in $B_{11}C_pCBC$, at the expense of transgranular fracture, is being investigated as a potential toughening mechanism. ARL/Johns Hopkins University (JHU) experiments have shown the presence of (101) twin boundaries in B_4C. Figure 8.2 shows a 96.3° tilt boundary as an example $B_{11}C_pCBC$ (101) twin boundary. One can see the bonds breaking as the grain boundary separates. Bulk dopants that segregate to the grain boundary may lower the fracture energy, thus promoting intergranular fracture. Dopants and impurities such as carbon (C), oxygen (O), Al, sulfur (S), Fe, and yttrium (Y) are currently under investigation. Preferred dopant bulk site locations have been found. DFT computations of $B_{11}C_pCBC$ grain boundary fracture energetics, with and without dopants, are underway and are expected to identify dopants that may enhance the intergranular fracture mechanism.

(a) **(b)**

(c) **(d)**

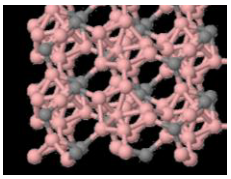

Fig. 8.2 $B_{11}C_pCBC$ (101) twin grain boundary at 96.3° tilt angle. (Angle showing bonds breaking at successively higher stress in a) through d).)

8.4 Collaborative Interactions

This project has involved extensive collaborations with researchers at ARL including, but not limited to, Gary Gilde, Jennifer Dunn, Todd Beaudet, Betsy Rice, Jerry LaSalvia, Bob Pavlacka, Gene Shanholtz, Steve Kilczewski, Gary

Gilde, Betsy Rice, and Jim McCauley. The theory group has been holding weekly teleconferences with Dr John Smith, and the experimental group has held approximately monthly meetings at JHU with Prof Hemker and his postdocs.

8.5 Publications and Presentations

None.

9. Administration, Education, Training, and Collaborative Structures

Hopkins Coordinator: KT Ramesh

ARL Coordinators: J McCauley, RJ Dowding

9.1 Long-Range Objectives

We aim to develop a collaborative research structure with significant educational benefits to both the US Army Research Laboratory (ARL) and Johns Hopkins.

9.2 Objectives for July 2011 to June 2012

Third Quarter 2011:

- Bring together ARL staff and Hopkins faculty and students in a Center Seminar.

Fourth Quarter 2011:

- Bring together ARL staff and Hopkins students and faculty in Collaborative Research Group meetings.

First Quarter 2012:

- Bring together ARL staff and Hopkins faculty and students in a Center Seminar.

Second Quarter 2012:

- Bring together ARL staff and Hopkins students and faculty in Collaborative Research Group meetings.

9.3 Accomplishments

The various groups are meeting regularly, and the seminar series is running well. Invited Center for Advanced Metallic and Ceramic Systems seminar speakers in this period are listed in the following Table:

SPEAKER	ABSTRACT	DATE
Patrick Michel	Numerical modeling of various processes affecting asteroids (disruption, spin-up, surface motions)	December 2, 2011
Angela Stickle	EPIC FAILURE: Examining Subsurface Damage Following Oblique Impacts	February 17, 2012
Marco Delbo	Temperature Shocks at the Origin of Regolith on Asteroids	April 6, 2012
Robert C Cammarata	Generalized Thermodynamics of Surfaces with Application to Small Solids	April 20, 2012
Gerald I Kerley	An Overview of Equation of State Modeling Techniques	June 4, 2012
Upadrasta Ramamurty	Fracture in amorphous alloys: Mechanisms and length scales	June 29, 2012

10. List of Theses, Publications, and Presentations

1. Williams C. PhD in Mechanical Engineering, date conferred 2012 May 21.
2. Taylor DE, Wright TW, McCauley JW. First principles calculation of stress induced amorphization in armor ceramics. Aberdeen Proving Ground (MD): Army Research Laboratory (US); 2012 Mar. Report No.: ARL-TR-5966.
3. Daphalapurkar NP, Hu G, Ramesh KT. Specimen size effects on the dynamic failure strength of brittle materials, ICACC; 2012 Jan; Daytona, FL.
4. Daphalapurkar NP, Ramesh KT. Designer materials for a secure future. Defense, Security and Sensing, SPIE, 2012.
5. Daphalapurkar NP, Wright TW, Ramesh KT. Dynamics of twin boundary motion in face-centered cubic metals. SES; 2011 Oct; Evanston, IL.
6. Daphalapurkar NP, Wright TW, Ramesh KT. Kinetics of moving twin boundaries. TMS; 2012 Mar; Orlando, FL.
7. Huskins EL. The thermo-mechanical response of UFG aluminum at high strain rates [dissertation]. [Baltimore (MD)]: The Johns Hopkins University; 2012.
8. Huskins EL, Ramesh KT. Microstructure evolution of UFG Al-1100 during high temperature Kolsky bar experiments. Session: Novel Testing Techniques II, SEM International Congress. 2012 Jun 11–14. Costa Mesa, CA.
9. Huskins EL. PhD in Mechanical Engineering, date conferred 2012 Aug 31.
10. Wright TW. Nonlinear anisotropic elasticity: guide for exploring stability in pressure/shear. Presented at the American Physical Society, 2012 Feb; Boston, MA.
11. Wright TW. Nonlinear elastic constitutive representations. Presented at Society of Engineering Science, 2011 Oct; Evanston, IL.
12. Taylor DE, Wright TW, McCauley JW. First principles calculation of stress induced amorphization in armor ceramics. Aberdeen Proving Ground (MD): Army Research Laboratory (US); 2012 Mar. Report No.: ARL-TR-5966.

Journal Articles

1. Daphalapurkar NP, Ramesh KT. Orientation dependence of the nucleation and growth of partial dislocations and possible twinning mechanisms in aluminum. J Mech Phys Sol. 2012;60:277–294.
2. Daphalapurkar NP, Patil S, Ramesh KT. On modeling BCC crystal plasticity: application to molybdenum. Manuscript for submission to Acta Materialia.
3. Daphalapurkar NP, Wright TW, Ramesh KT. Kinetics of a fast moving twin boundary. Manuscript for submission to Physical Review Letters.
4. Huskins EL, Cao B, Li B, Ramesh KT. Temperature-dependent mechanical response of an UFG aluminum alloy at high rates. Experimental Mechanics. 2012;52:185–194.
5. Wright TW. Bootstrap Elasticity: From Linear to Nonlinear Constitutive Representations. Journal of Elasticity. 2012;109(1):35–49.
6. Daphalapurkar NP, Ramesh KT. Orientation dependence of the nucleation and growth of partial dislocations and possible twinning mechanisms in aluminum. J Mech Phys Sol. 2012;60:277–294.
7. Huskins EL, Cao B, Li B, Ramesh, KT. Temperature-dependent mechanical response of an UFG aluminum alloy at high rates. Experimental Mechanics. 2012;52:185–194.
8. Wright TW. Bootstrap elasticity: from linear to nonlinear constitutive representations. Journal of Elasticity. 2012;109(1):35–49.
9. Daphalapurkar NP, Patil S, Ramesh KT. On modeling BCC crystal plasticity: application to molybdenum. Manuscript for submission to Acta Materialia.
10. Daphalapurkar NP, Wright TW, Ramesh KT. Kinetics of a fast moving twin boundary. Manuscript for submission to Physical Review Letters.

Presentations

1. Daphalapurkar NP, Hu G, Ramesh KT. Specimen size effects on the dynamic failure strength of brittle materials. ICACC, 2012 Jan; Daytona, FL.
2. Daphalapurkar NP, Ramesh KT. Designer materials for a secure future. Defense, Security and Sensing, SPIE., 2012.
3. Daphalapurkar NP, Wright TW, Ramesh KT. Dynamics of twin boundary motion in face-centered cubic metals, SES, 2011 Oct; Evanston, IL.

4. Daphalapurkar NP, Wright TW, Ramesh KT. Kinetics of moving twin boundaries. TMS, 2012 Mar; Orlando, FL.

5. Huskins EL, Ramesh KT. Microstructure evolution of UFG Al-1100 during high temperature kolsky bar experiments. Session: Novel Testing Techniques II, SEM International Congress. 2012 Jun 11–14; Costa Mesa, CA.

6. Wright TW. Nonlinear anisotropic elasticity: guide for exploring stability in pressure/shear. Presented at the American Physical Society, 2012 Feb; Boston, MA.

7. Wright TW. Nonlinear elastic constitutive representations. Presented at Society of Engineering Science, Oct 2011; Evanston, IL.

1 (PDF) DEFENSE TECHNICAL INFORMATION CTR
DTIC OCA

2 (PDF) DIRECTOR
US ARMY RESEARCH LAB
RDRL CIO LL
IMAL HRA MAIL & RECORDS MGMT

1 (PDF) GOVT PRINTG OFC
A MALHOTRA

49 (7 HC, 42 PDF) DIR USARL
RDRL CIH C
P CHUNG
D GROVE
J KNAP
RDRL WM
P BAKER
B FORCH
J MCCAULEY (6 HC)
P PLOSTINS
RDRL WML B
I BATYREV
B RICE
D TAYLOR
N WEINGARTEN
RDRL WML H
B SCHUSTER
RDRL WMM
J BEATTY
R DOWDING
J ZABINSKI
RDRL WMM B
G GAZONAS
RDRL WMM E
C HILTON
S KILCZEWSKI
J LASALVIA
P PATEL
J SINGH
J SWAB
RDRL WMP
S SCHOENFELD
RDRL WMP B
C HOPPEL
D POWELL
S SATAPATHY
M SCHEIDLER
T WEERASOORIYA
RDRL WMP C
R BECKER
S BILYK
T BJERKE
D CASEM
J CLAYTON (1 HC)
D DANDEKAR
M GREENFIELD
R LEAVY
M RAFTENBERG
S SEGLETES
C WILLIAMS
RDRL WMP D
R DONEY
RDRL WMP E
S BARTUS
RDRL WMP F
N GNIAZDOWSKI
RDRL WMS
M VANLANDINGHAM

INTENTIONALLY LEFT BLANK.